

# Primary Structure for a CubeSat 1U for QKD applications: Design and Analysis

Josué Aarón López Leyva, *Member, IAENG*, Dalia Holanda Chávez García, Felipe Choza Torrecillas, Ariana Talamantes Álvarez, Miguel Ángel Ponce Camacho.

**Abstract**—An optimized primary structure for CubeSat 1U for QKD application is presented. Several proposals are shown where each one was analyzed regarding the mass quantity, natural frequency, thermal distribution and static forces based on the finite element computational method. The simulation results show that the optimized structure presents a mass of 155.43 gr using Al 7075 T6 (meaning a reduction of 50% compared to the initial model), natural frequency of 1204.9Hz, amplitude variations of 16.5 mm and that the general thermal distribution remain constant  $\approx 79$  °C under extreme thermal range, -13 °C – 136 °C. These results allow an adequate internal environment for a particular performance of an optical payload for QKD applications based on a reduced thermal noise.

**Index Terms**—CubeSat, thermal analysis, optimization, structure

## I. INTRODUCTION

Nowadays, small satellites are widely used for different applications, such as the security systems around the world. In particular, a novel and suitable security option that provides unconditional security are the Quantum Key Distribution (QKD) systems [1]-[5]. Thus, by combining the spacecraft technology and quantum secure systems, it is possible to propose QKD applications based on QKD payload using the CubeSat standard (i.e. mainly, 10 cm x 10 cm x 10 cm of dimension, mass 1-1.33 Kg) [6], [7]. However, both spacecraft and QKD technologies have particular issues and trade-offs that have to be solved in order to increase the performance of these hybrid systems, i.e. QKD systems implemented in CubeSat. In this case, it is not considered a strict analysis of the design requirements and performance parameters for QKD systems (although can be found in [8], [9]), but in general, these requirements are highly related to the internal volume available in the CubeSat, thermodynamical and electrostatic effects, optimum structure, among others. Thus, in general, the mass quantity, material kind used and material deformation (shape or size) due to the vibrations and forces (presented during

the launching process and other stages) are parameters that have to be considered in order to optimize a mechanical structure design and CubeSat manufacturing. Thus, a proper functioning (protects the system's integrity) and performance of secure communication mission have to be ensured, because otherwise, an inadequate structure design can cause damages, for example, to the Acquisition, Tracking and Pointing (ATP) system and linewidth of the laser used for both classical and quantum optical communications [10], [11]. In fact, if a CubeSat structure presents an important material deformation due to the external forces applied, the direct communication link between the CubeSat and the ground station will be difficult, because there is not trusted location reference and other systems and algorithms will be needed as coarse and fine countermeasures [12], [13]. In this paper, the optimum design and analysis for a primary CubeSat structure for QKD application is presented. This optimum design is based on the optimization of several designs and performance parameters considering a CubeSat 1U. In fact, this paper is focused on the mechanical structure of CubeSat, remarking that, if it does not satisfy particular design and manufacturing parameters, the overall performance of QKD systems will be degraded. This paper is organized as follows: Section II presents the theoretical background regarding the analysis of the CubeSat structure. Section III shows the proposals of structural design and simulation results. In addition, this section presents an analysis of the results and the conclusion is given in Section IV.

## II. THEORETICAL BACKGROUND

### A. Combined Load Factor Analysis

The CubeSat structure has diverse loads generated due to a combination of states (e.g. stable state, low-frequency transient state, and high-frequency vibro-acoustic charges state) presented at the complete launching process. Thus, it is necessary to calculate the combined load factors for any stage of the launching process in order to design the optimal structure that can support these combined loads. In particular, there are considered the combined load factor ( $N_i$ ), steady state load factor ( $S_i$ ), low frequency dynamic load factor ( $L_i$ ) and the load factor due to the high frequency random vibrations ( $R_i$ ), where each factor is concerning to particular  $i$ -th axis (i.e.  $x$ ,  $y$ , and  $z$ -axis). These factors are related as Eq. (1) shows.

$$N_i = S_i \pm \sqrt{(L_i)^2 + (R_i)^2} \quad (1)$$

Manuscript received October 15, 2018; revised July 15, 2019. This work was supported in part by the Center of Innovation and Design.

Josue Aaron Lopez Leyva is with CETYS University, Ensenada, B.C. 22860 Mexico (phone: +52 (646) 174-50-95 ext. 140; e-mail: josue.lopez@cetys.mx).

Dalia Holanda Chavez Garcia is with CETYS University, Ensenada, B.C. 22860 Mexico (e-mail: dalia.chavez@cetys.mx).

Felipe Choza Torrecillas is with CETYS University, Ensenada, B.C. 22860 Mexico (e-mail: ing.felipechoza@gmail.com).

Ariana Talamantes Álvarez is with CETYS University, Ensenada, B.C. 22860 Mexico (e-mail: ariana.talamantes@cetys.edu.mx )

Miguel Angel Ponce Camacho is with CETYS University, Mexicali, B.C. 21259 Mexico (e-mail: miguel.ponce@cetys.mx)

The results obtained using Eq. (1) (i.e.  $N_x$ ,  $N_y$  and  $N_z$ ), should be considered as if they were acting simultaneously in all possible combinations. In fact, this load combinational process can be interpreted and related with the forces and stress values produced by these factors. Considering the last, the load factors that affect in direct way the mechanical vibrations will be analyzed. Thus, the factors for the combined loads applied to the small satellite structure were calculated in order to apply the boundary conditions using the Finite Element Method (FEM). In particular, the total load ( $N_T$ ) of a CubeSat is described by Eq. (2).

$$N_T = \sqrt{(N_x)^2 + (N_y)^2 + (N_z)^2} \quad (2)$$

, where the  $N_x$ ,  $N_y$  and,  $N_z$  values are the particular components of the  $N_T$  parameter. The combined load factor ( $N_T$ ) allows an approximation to the real value of the loads applied to the satellite during the takeoff of the launch vehicle [14], [15]. In addition, assuming that the satellite is placed according to its longitudinal axis parallel to the launch vehicle, it can be assumed that the loads are in the support points of the satellite structure. Next, the particular launcher selection is needed in order to determine the values of the parameters used in Eq. (1), i.e. each launcher has particular values parameters commonly considering the gravitational force ( $g$ ) as unit of measure. In our case,  $N_T \approx 30$  N (conversion based on  $g$  values for each parameter used in Eq. (1) considering the satellite mass used). Based on FEM analysis, the forces are calculated considering the Eq. (3), where  $M$  is the mass matrix,  $C$  is the damping matrix,  $K$  is the stiffness matrix,  $F$  is the nodal forces vector,  $\omega$  is the angular frequency nodal and  $u$  is the nodal displacement vector, considering that the first and second derivative meaning the nodal velocity and acceleration, respectively [16].

$$[M]\{\ddot{u}\} + [C]\{\dot{u}\} + [K]\{u\} = \{F\}e^{j\omega t} \quad (3)$$

In particular, the static analysis is obtained without considering the time dependency of the structural analysis, i.e. nodal velocity and acceleration values are zero. Thus, the  $N_T$  value can be considered as the satellite force, which it has to be moved or launched using a higher force depending on the principal ( $\approx 44$  N) and thrower ( $\approx 57$  N) springs implemented in CubeSat deployer systems, in our case, 1U CubeSat deployer system. It is important to clarify that, if more CubeSat units are needed,  $N_T$  is remains constant for each unit but the force needed to move all CubeSat units is directly proportional to the structure amount, and thus, the principal and thrower springs forces are increased. Therefore, the force needed to deploy the CubeSat 1U is  $\approx 660$  N. Considering the boundary conditions that were raised for the analysis of vibrations in this project, the main structure of the CubeSat is supported in eight points that are assumed as the lower and upper regions of the rails or areas of union between the structure and the launcher. Thus, a safety factor (2.5) is used, so the force will be  $\approx 1,650$  N. However, this force is applied to four support points, so the particular force for each support point is  $\approx 416$  N.

### B. Thermal analysis

The dynamical thermal conditions of the space environment affect the CubeSat structure temperature, and in the same way, the structure temperature affects the performance of the systems implemented inside the satellite structure [17]. Thus, electronic noise caused by thermal variations is called Johnson–Nyquist noise [18]. In particular, the Root Mean Square (RMS) voltage ( $v_n$ ) generated by thermal conditions is described by Eq. (4).

$$v_n = \sqrt{4k_B T R \Delta f} \quad (4)$$

, where  $k_B$  is the Boltzmann's constant ( $\approx 1.38 \times 10^{-23}$  J/ $^0$ K),  $T$  is the absolute temperature in Kelvin degrees,  $R$  is the resistance value and  $\Delta f$  is the bandwidth of the element, material or systems analyzed. It is well-known that a CubeSat needs an internal thermal control system in order to maintain a quasi-constant temperature so as not to degrade the performance of the subsystems implemented [19]. However, thermal analysis of the structure is also important in order to relax the requirements of the thermal control system and improve energy efficiency. In this case, it is important that the temperature structure is not affected by the external temperature, i.e. the structural design has to provide a temperature distribution without extreme variations.

## III. DESIGNS AND SIMULATION RESULTS

The optimized structure design of a CubeSat, as well as the frequency and thermal testing simulations results, are shown. Firstly, a simple design is carried out and next it is optimized in order to reduce the mass without losing structure rigidity. The SolidWorks (SW) 2017 premium software is used in order to perform these simulations. In addition, a static force analysis was performed considering the safety factor that specified each simulation condition in order to maintain an adequate design optimizing the mass quantity.

### A. Basic Model

A basic model of the CubeSat structure is created taken into account only the inputs ports and holes for the assembly as shown in Fig. 1a) and 1b).

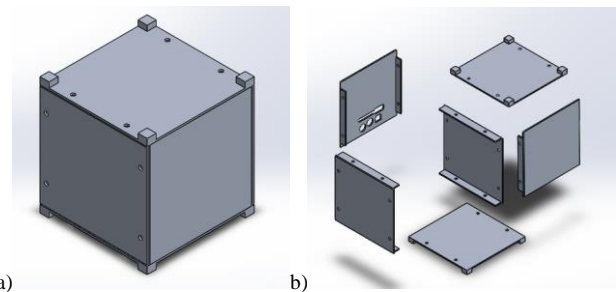


Fig. 1. a) SolidWorks assembly model in isometric view which shows that no cut was made to reduce mass, b) Exploded view of the 6 pieces of the assembly.

Next, static analysis is performed in order to monitor the forces at the initial mode. In particular, a fixed grip is made on the four lower support points since our CubeSat is supported by these and a force of 416 N is applied in each

four upper support points as shown in Fig. 2. This force value is based on the combined load factors calculation. It can be seen that maximum stress of 16,695 MPa is obtained as a result of our static analysis and, considering that the tensile strength is 570 MPa, it is possible to ensure that our model will resist the forces applied.

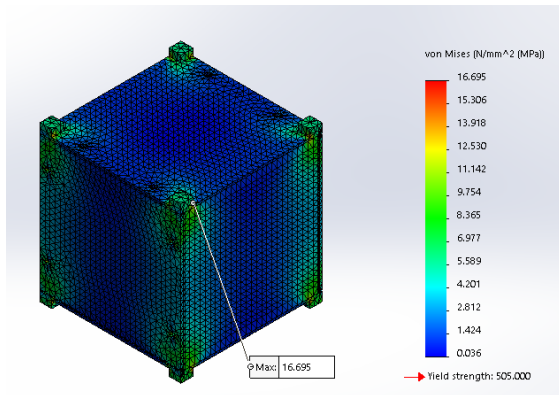


Fig. 2. Static analysis of the first model.

Then, frequency analysis for the initial model is performed considering that the model only is moving on a single axis due to the restraints that it presents when it is transferred to the orbit. Therefore, a fixed grip is made on its four lower supports and a sliding grip is considered on the lateral faces of the upper supports in order to help the single axis displacement. In addition, the calculated load (i.e. 416 N) is applied to each of the upper supports as shows Fig. 3.

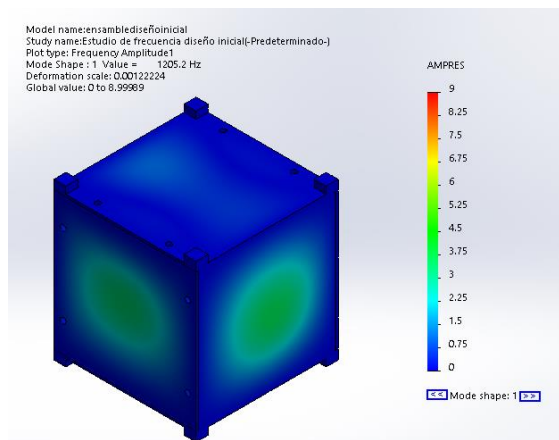


Fig. 3. Frequency analysis of initial model at 1205.2 Hz.

The AMPRES (Resultant Amplitude) measure described in the figure is used refer to the wave amplitude (millimeter, mm). In particular, the natural or resonant frequency result is 1205.2 Hz and 9 mm for maximum amplitude, meaning that these values are in the frequencies range allowed. In addition, Fig. 4a), 4b) and 4c) shown that the point of maximum amplitude is in the central part of the face, where the cuts were made (taking into account that red and blue color indicates maximum and minimum values, respectively) and that the maximum amplitude concentration is located in the central points of the face as well. These observations indicate that the central points of the face are an ideal starting point to begin removing mass from the model, without losing the main objective which is the reduced mass while the mechanical properties effects are minimum as possible.

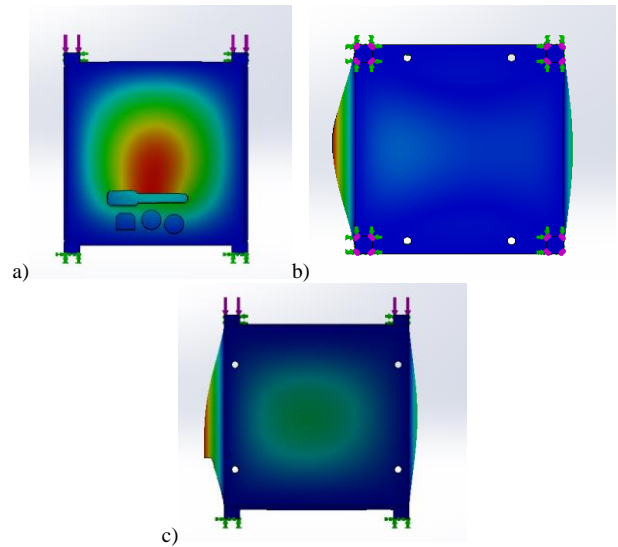


Fig. 4. Frequency analysis results. a) front part, where the maximum amplitude point was obtained. b) top view of the model, all the displacement obtained in the front face is observed. c) side view of the model is observed as the maximum area the center of the face.

Next, thermal analysis is carried out considering several factors to obtain a better simulation of the model. It is important to take into account the temperature factor in the study of our model, i.e. as it will be affected by space conditions in orbit. In particular, aluminum emissivity is 0.05, radiation temperature (which is emitted by the sun's rays) is applied on the front face, 136 °C, and a radiation temperature of -13 °C is applied to the rear face, which is in the shade side, as shown in Fig. 5. As observed, the maximum temperature is 87 °C.

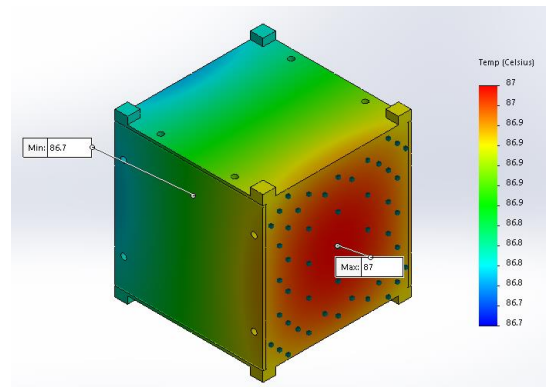
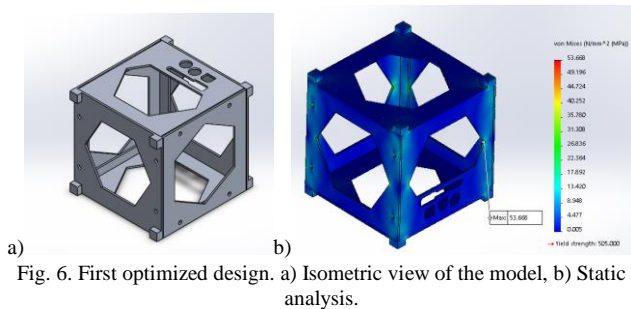


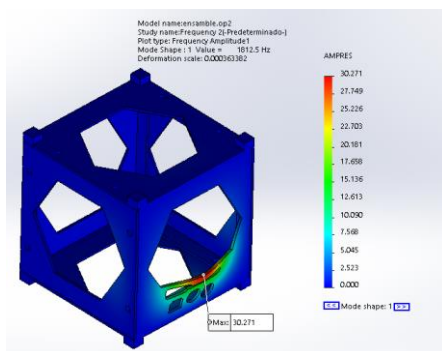
Fig. 5. Thermal analysis results.

### B. First Optimized Design

By analyzing the results of the simulations performed on the initial model, it is observed that the central part of the faces presents the greatest frequency amplitudes which indicate that it is the best point to remove the mass. Hence, it is proposed to make a hexagon cut in each of the faces as Fig. 6a) shows, thereby reducing from 311 to 200 gr (i.e. regarding initial and first optimized model, respectively), achieving the removal of 35% of the mass of the initial design.



First, static analysis is performed to find the maximum effort. In the same way, the four fixed lower supports and the force applied in the upper supports (416 N in each of them) were considered. It was found that the maximum stress is 53,668 MPa, which is greater than the obtained in the initial design but remains low with respect to the tensile strength that our material can withstand. In addition, it can be seen that the mass reduction with this specific configuration of hexagons results in an increase in the stresses. The maximum point of effort shown in Fig. 6b) is found on the side where the cuts for the connection ports are located. The results show that this design modification is not optimal and that it will be necessary to redesign in a way in which the mass removal does not increase the stresses. Next, a frequency analysis is performed taking into account the considerations described above: lower supports fixed, upper supports with slider restriction and force applied in the upper part (416 N in each support), as Fig. 7 shows. Thus, the reduction mass was 65% respect to the initial mass but at the same time, the model lost rigidity which caused that the stress increases. The natural or resonant frequency and amplitude increased, 1812.5 Hz and 30.271 mm, respectively, due to the loss of mass and stiffness of the model, so it is advisable to research for a different configuration that gives better results.



Lastly, the thermal simulation is carried out (see Fig. 8) taking into account the aforementioned temperatures: a maximum of 136 °C and a minimum of -13.15 °C. It is observed that the minimum and maximum temperatures are 86,679 °C and 86,942 °C, respectively.

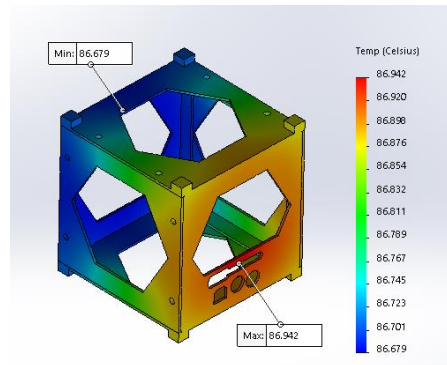


Fig. 8. Thermal analysis.

C. Second Optimized Design

A second optimized design is made considering as starting point the initial design, but with the feedback that generated the first optimized design, where it was observed that when removing all the mass from the center of the faces, rigidity is also reduced and the frequency and amplitude are increased. Thus, a design was made in which mass was removed in the central point of the faces, as well as in its corners. The largest mass cut was made on the upper and lower face as shown in Fig. 9a) since in our past simulations was observed that they are usually the least affected points. These modifications allow a mass reduction with 173 gr. of final mass, which means 55% of the total mass (in other words, a reduction of 45%). Following the procedure performed in the initial model as well as in the first optimized model, the static analysis is firstly performed (see Fig. 9b)) in order to monitor the stress considering the mass reduction. The four fixed lower supports and the force of 416 N applied in the upper supports are considered. The results show that maximum stress of 32,986 MPa is obtained, which is a decrease of 21 MPa with respect to the first optimized model. Although the mass was reduced with respect to the previous design, it gained rigidity. This means that this configuration can still be improved.

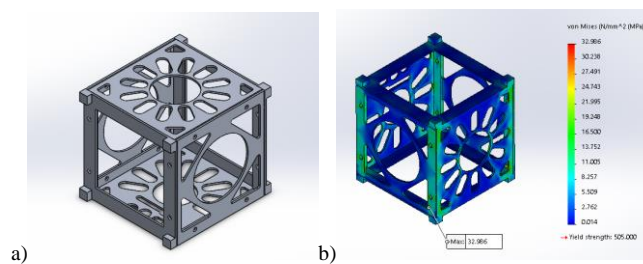


Fig. 9. Second optimized model. a) Isometric view of the second optimized model, b) Static analysis of the second optimized design.

Next, the frequency analysis is performed (see Fig. 10) with the same restrictions considered previously. The results show a resonant frequency and amplitude of 1239.5 Hz and 15.9 mm, respectively, which is a remarkable improvement over the previous design, showing a reduction in frequency, amplitude and mass. Even with the results improved, it is still proposed to lower the mass and continue to increase rigidity in the model.

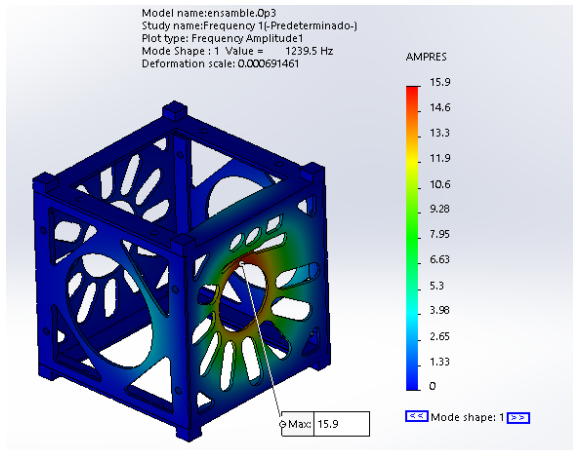


Fig. 10. Frequency analysis of second optimized design at 1239.5 Hz.

Then, the thermal analysis was done considering the aforementioned parameters and the heat transfer by radiation as shown in Fig. 11. The results show a maximum of 82.6 °C and a minimum of 82.2 °C. In particular, it remains a temperature that will not affect our model due to the physical properties of the material used.

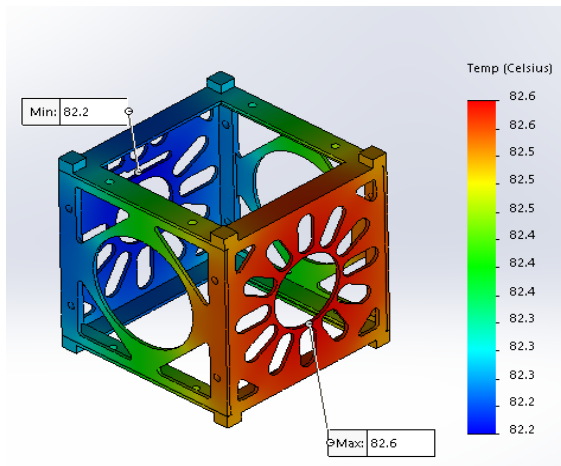


Fig. 11. Thermal analysis of the second optimized design.

**D. Final Optimized Model**

An optimized final design is proposed based on the previous designs as feedback. The material extraction is performed in central parts, but support is left as shown in Fig. 12a), in order to avoid extremely stiffness reduction in our model. With this proposal, a final material reduction was achieved, reaching 155 grams, which is 50% of the total mass of the initial model. This reduction is really important since all that mass can be replaced for a particular payload according to the CubeSat mission.

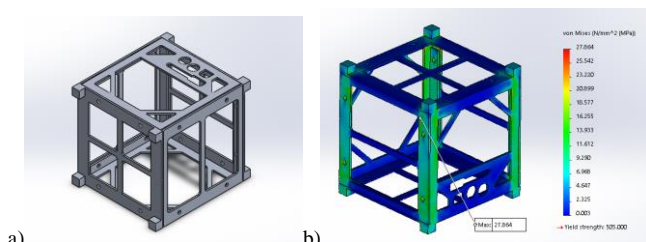


Fig. 12. Final Optimized model. a) Isometric view of final design, b) Static analysis of the final design.

The static analysis is performed in order to obtain the results of the final design (see Fig. 12b)), considering the restrictions as well as the four fixed lower supports and the force applied in the upper supports. Thus, the maximum stress is decreased, almost reaching the value of the initial model, but with half the mass. The maximum value reached is 27.86 MPa which shows the stress reduction, in the same way that mass is reduced, the cuts are configured to support our design. Then, a frequency analysis is performed as shown in Fig. 13 considering the restrictions and applied forces. The results show a natural resonant frequency and amplitude of 1204.9 Hz and 16.5 mm, respectively. It is observed that in the final optimized model the natural frequency is possible to reduce, however, the amplitude increases 1 mm, which can be negligible when obtaining a better resistance to stress, a reduction of mass and a lower frequency.

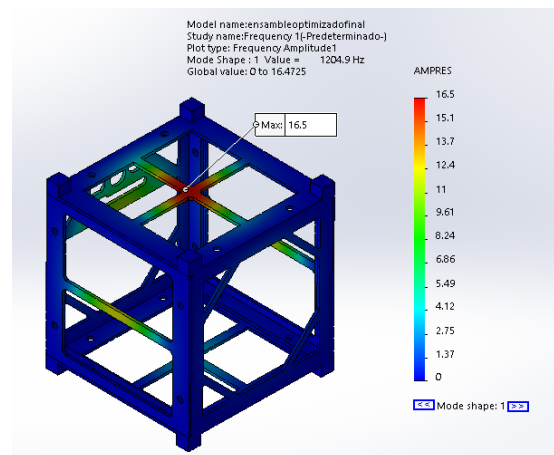


Fig. 13. Frequency analysis at 1204.9 Hz.

Fig. 14 shows the simulation results of the temperature analysis to observe how the model behaves with the mass reduction and the new configuration. It can be seen that when reducing mass, the temperature is leveled at lower values, resulting in a maximum of 77.3 °C and a minimum of 77 °C, which means that the temperature will not affect significantly the performance model.

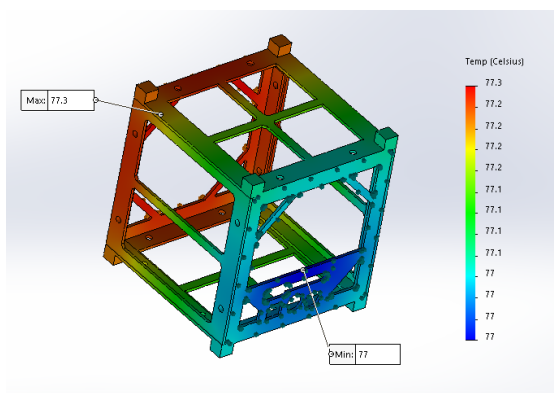


Fig. 14. Thermal analysis of the final optimized design.

Once the results are obtained in a particular way, it is important to concentration the data in order to make a comparison (see Table I).

TABLE I  
 UNITS FOR MAGNETIC PROPERTIES

Parameter	Model #1	Model #2	Model #3	Model #4
Mass (gr)	311	200.26	173.43	155.43
% mass	100	64.37	55.7	50
Strength (MPa)	16.7	53.67	32.99	27.86
Freq. (Hz)	1205.2	1812.5	1239.5	1204.9
AMPRES (mm)	9	30.3	15.9	16.5
Temp. Min (°C)	86.7	86.68	82.2	79.11
Temp. Max (°C)	87	86.94	82.6	78.61

Now, the basic and optimized structures were analyzed (i.e. worst and better case, respectively) regarding the voltage noise signal generated described by Eq. (4) considering an  $R = 50 \Omega$ ,  $\Delta f = 100 \text{ MHz}$  and the extreme temperature sides, hot and cold side (hot and cold case, respectively) in the satellite design context.

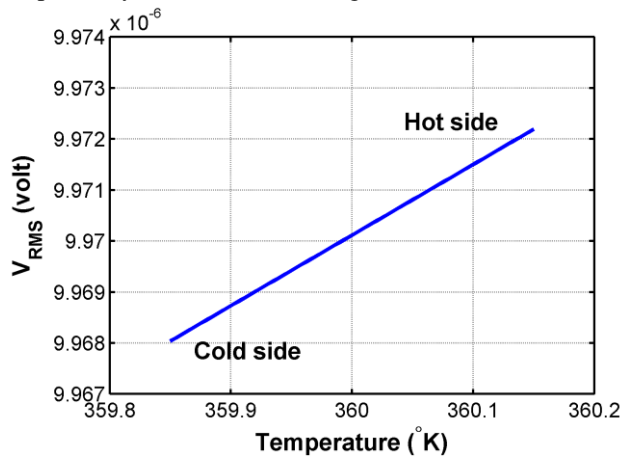


Fig. 15.  $V_{RMS}$  generated by thermal noise based on the thermal distribution in the first structure proposed.

Fig. 15 shows the noise signal generated due to the thermal distribution in the CubeSat structure, where it is possible to observe that for the hot side, the  $V_{RMS}$  value is higher ( $\approx 9.972 \mu\text{V}$ ) than the noise value at the cold side ( $\approx 9.968 \mu\text{V}$ ). The reason for the last is because the first structure proposed have more mass quantity than the optimized structure. Fig. 16 shows the noise signal generated for the optimized structure, where it is possible to observe that the  $V_{RMS}$  value is decreased for both hot (from  $\approx 9.972 \mu\text{V}$  to  $\approx 9.837 \mu\text{V}$ ) and cold side (from  $\approx 9.968 \mu\text{V}$  to  $\approx 9.833 \mu\text{V}$ ) of the CubeSat structure.

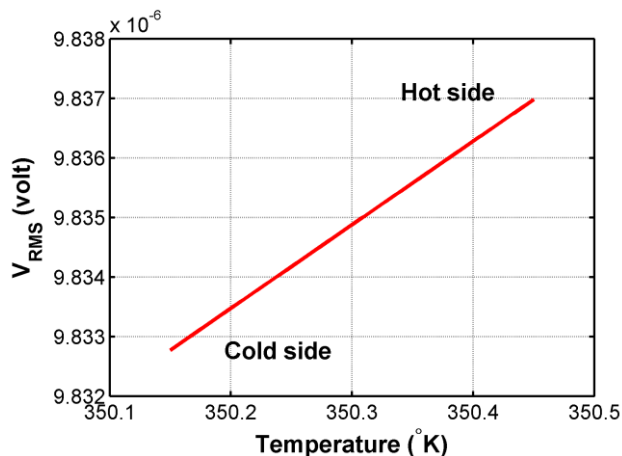


Fig. 16.  $V_{RMS}$  generated by thermal noise based on the thermal distribution in the optimized structure proposed.

In order to clarify, the results showed regarding the thermal noise in both basic and optimized structures are calculated using particular parameters values (i.e.  $R = 50 \Omega$ ,  $\Delta f = 100 \text{ MHz}$ ). However, for real QKD application using CubeSat, several electronic instrumentations are used at different frequencies and bandwidth. For example, Ultra High Frequency (UHF) and Super High Frequency (SHF) bands are very useful radio band frequencies for conventional communication in satellite links, which working from 300 MHz to 30 GHz. Thus, the effect of these communication modules (based on UHF and SHF) regarding the thermal noise generated by the thermal distribution in the satellite structure is critical. Finally, Fig. 17 shows the Bit Error Rate (BER) measurement in the laboratory for the minimum and maximum temperature. As can be seen, the optimized structure allows reducing the BER ( $\approx 1 \times 10^{-9}$ ) with respect to the first structure ( $\approx 35 \times 10^{-9}$ ). This means that the optimized design increases the performance of the CubeSat.

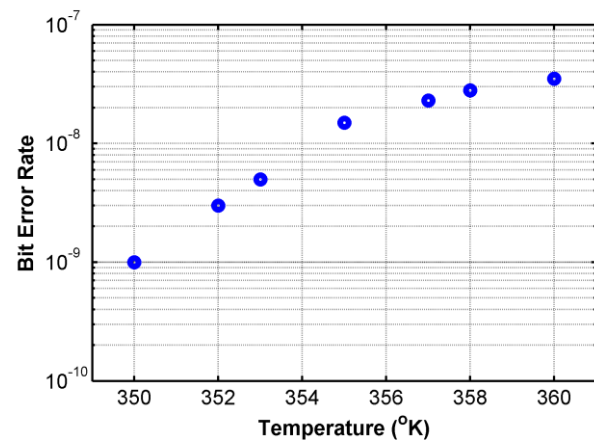


Fig. 17. Bit Error Rate considering the maximum and minimum temperature for first and for optimized structure

#### IV. CONCLUSION

Quantum Key Distribution systems based on CubeSat communication links require a detailed design regarding overall systems and structures to improve the overall performance in order to establish a secure communication system for all users. In particular, the mass reduction allows the inclusion of more subsystems contributing to the overall performance, such as, energy subsystems to increase the lifetime of the project in orbit, high-end digital processing units that require more energy, tracking-acquisition-pointing subsystem, among others. In this paper, an optimized structural mechanical design of a CubeSat is presented. The material used for the simulation was Al 7075 T6. Four structural designs were developed in which static force and thermal analysis were performed in order to determine the best performance under real conditions. It is observed that our simulated model is one piece, which is the one with the least mass of all, and the lowest frequency. As mentioned above, if the mass decreases, the frequency increases as long as the rigidity of the system remain constant. In addition, the model mass is reduced, but in the same way, rigidity is reduced in the system, which implies a lower frequency. The results about the mechanical structure are important in order to continue the manufacturing process and perform several

testing needed (e.g. functionality, vibration, mechanical shock, thermal cycling, thermal vacuum, total ionizing dose, among others). In particular, a mass reduction of 62.6% was obtained, i.e. the final structure mass was 37.4% considering the initial mass. Additionally, an increase in the force structure was achieved from 16.7 MPa to 41.7 MPa for initial and optimized structure, respectively. On the other hand, the frequency analysis shows that the optimized structure design has a small physical region with vibrations effects; however, these results help to strategically place mass elements (subsystems) in the CubeSat. The frequency analysis allows determining the possible geometry change and analyzing the shock isolators performance. Finally, the optimum design allows a multiple Printed Circuit Board (PCB) mounting configurations, maximum flexibility, and security for the systems mounted, although the secondary structure is not presented in this paper because it is related with a particular space mission.

## REFERENCES

- [1] R. Bedington, J. M. Arrazola and A. Ling, "Progress in satellite quantum key distribution", *NPJ Quantum Information*, vol. 3, no. 30, pp.1-13, August 2017.
- [2] G. Vallone, et al., "Experimental satellite quantum communications", *Physical Review Letters*, vol. 115, pp. 1-5, July 2015.
- [3] J. Yin, et al., "Satellite-based entanglement distribution over 1200 kilometers", *Science*, vol. 356, pp. 1140-1144, June 2017.
- [4] D. K. Oi, et al., "CubeSat quantum communications mission", *EPJ Quantum Technology*, vol. 4, no. 6, pp.1-20, December 2017.
- [5] S.-K. Liao, et al., "Long-distance free-space quantum key distribution in daylight towards inter-satellite communication", *Nature Photonics*, vol. 11, pp. 509-513, July 2017.
- [6] J. A. Grieve, R. Bedington, Z. Tanga, R. Chandrasekara, A. Lingab, "SpooQySats: CubeSats to demonstrate quantum key distribution technologies", *Acta Astronautica*, vol. 151, pp. 103-106, October 2018.
- [7] E. Kerstel, et al., "Nanobob: A CubeSat mission concept for quantum communication experiments in an uplink configuration", *EPJ Quantum Technology*, vol. 5, no. 6, June 2018.
- [8] R. Bedington, et al., "Nanosatellite experiments to enable future space-based QKD missions", *EPJ Quantum Technology*, vol. 3, no. 12, pp. 2-10, October 2016.
- [9] J-P. Bourgoin, et al., "A comprehensive design and performance analysis of low Earth orbit satellite quantum communication", *New Journal of Physics*, vol. 15, pp.1-35, February 2013.
- [10] J-H, Wang, et al., "Direct and full-scale experimental verifications towards ground-satellite quantum key distribution", *Nature Photonics*, vol. 7, pp. 387-393, April 2013.
- [11] D. He, et al., "Acquisition technology for optical ground stations in satellite-ground quantum experiments", *Applied Optics*, vol. 57, no. 6, pp. 1351-1357, 2018.
- [12] Y. Kaymak, et al., "A Survey on Acquisition, Tracking, and Pointing Mechanisms for Mobile Free-Space Optical Communications", *Communications Surveys & Tutorials*, vol. 20, no. 2, pp. 1104 - 1123 2018.
- [13] J. Tan, et al., "All-Optical Transparent Forwarding Relay System for Interstellar Optical Communication Networks", *Journal of Quantum Electronics*, vol. 54, no. 2, pp. 1-7, April 2018.
- [14] A. Girard and N. Roy, *Structural Dynamics in Industry*, J. Wiley and Sons, 2008, ch. 11.
- [15] J. Wijker, *Mechanical Vibrations in Spacecraft Design*, Springer, 2004, ch. 1.
- [16] J. N. Reddy, *An Introduction to the Finite Element Method*, 3rd ed. New York: McGraw-Hill, 2006, ch. 3.
- [17] M. Gadalla, "Prediction of temperature variation in a rotating spacecraft in space environment." *Applied Thermal Engineering*, vol. 25, no. 14-15, pp. 2379-2397, February 2005
- [18] P. Santagati and V. Beiu "Will thermal noise affect nano-communications?", *International Conference on Communications, Signal Processing, and their Applications (ICCSPA)*, pp. 1-4, United Arab Emirate, March 2013.
- [19] G. C. Birur and T. P. O'Donnell, "Advanced thermal control technologies for space science missions at Jet Propulsion Laboratory", *AIP Conference Proceedings*, vol. 552, no. 1, pp. 263-270, April 2001.